BIOMIMETICS

Bioinspired, ingestible electroceutical capsules for hunger-regulating hormone modulation

Khalil B. Ramadi[1,2,3,4,5]†*, James C. McRae[1,3]†, George Selsing[1], Arnold Su[1], Rafael Fernandes[1], Maela Hickling[6], Brandon Rios[1], Sahab Babaee[1,2,3], Seokkee Min[1], Declan Gwynne[1]‡, Neil Zixun Jia[1], Aleyah Aragon[1], Keiko Ishida[1,2,3], Johannes Kuosmanen[1,2,3], Josh Jenkins[1,2,3], Alison Hayward[1,3,7], Ken Kamrin[1], Giovanni Traverso[1,2,3]*

The gut-brain axis, which is mediated via enteric and central neurohormonal signaling, is known to regulate a broad set of physiological functions from feeding to emotional behavior. Various pharmaceuticals and surgical interventions, such as motility agents and bariatric surgery, are used to modulate this axis. Such approaches, however, are associated with off-target effects or post-procedure recovery time and expose patients to substantial risks. Electrical stimulation has also been used to attempt to modulate the gut-brain axis with greater spatial and temporal resolution. Electrical stimulation of the gastrointestinal (GI) tract, however, has generally required invasive intervention for electrode placement on serosal tissue. Stimulating mucosal tissue remains challenging because of the presence of gastric and intestinal fluid, which can influence the effectiveness of local luminal stimulation. Here, we report the development of a bioinspired ingestible fluid-wicking capsule for active stimulation and hormone modulation (FLASH) capable of rapidly wicking fluid and locally stimulating mucosal tissue, resulting in systemic modulation of an orexigenic GI hormone. Drawing inspiration from *Moloch horridus,* the "thorny devil" lizard with water-wicking skin, we developed a capsule surface capable of displacing fluid. We characterized the stimulation parameters for modulation of various GI hormones in a porcine model and applied these parameters to an ingestible capsule system. FLASH can be orally administered to modulate GI hormones and is safely excreted with no adverse effects in porcine models. We anticipate that this device could be used to treat metabolic, GI, and neuropsychiatric disorders noninvasively with minimal off-target effects.

INTRODUCTION

The extensive enteric nervous system (ENS), which controls the function of the gastrointestinal (GI) tract, is an important component of the gut-brain axis (*1*). The ENS is composed of the myenteric and submucosal plexuses, found in the muscular and submucosal GI tissue, respectively. Extrinsic neurons transmit signals back to the central nervous system via vagal and dorsal root ganglia afferents (*2*, *3*). Neuromodulation of ENS and afferent fibers occurs via various mechanisms, including direct neurocrine, endocrine, paracrine, and immune-mediated pathways (*3*, *4*), and has been primarily accomplished using pharmacotherapy and surgical interventions. These methods each carry their own limitations. Pharmaceuticals carry potentially severe off-target effects and can require painful modes of delivery, such as needles, that limit patient compliance. Surgical interventions often require invasive procedures associated with extended recovery times and increased risk to the patient. Electrical stimulation has attracted interest as a mechanism to leverage endogenous circuitry to modulate physiology through the activation or inhibition of nerves (*3*). Electrical stimulation enables higher-resolution spatial and temporal targeting than systemically administered pharmacotherapies to mitigate unwanted off-target effects. It can be applied to specific nerves and delivered over seconds to minutes.

Gastric electrical stimulation (GES) is one of the few commercially established GI electroceutical interventions to date and is Food and Drug Administration (FDA) approved for gastroparesis under a Humanitarian Device Exemption (*5*). Gastroparesis is a condition that arises because of delayed gastric emptying (defined as greater than 10% of a meal remaining 4 hours after ingestion). The clinical presentation of gastroparesis is heterogenous across patients. Some patients report uncontrolled emesis and ultimate dehydration, whereas others experience bloating and postprandial dyspepsia (*6*). Although the etiology of gastroparesis remains unknown, it occurs more frequently in people with diabetes and likely arises because of neuropathy (*7*). GES systems are subcutaneously implanted and contain electrodes that are surgically sutured to the gastric serosal surface (*8*). GES systems are similar to a cardiac pacemaker and are used to treat gastroparesis by applying short-pulse, high-frequency (0.3 ms, 14 Hz) electrical impulses. Studies have repeatedly shown that gastric emptying time is not reduced in patients with implanted GES systems (*9*). These patients do, however, experience a notable reduction in symptoms, including nausea and vomiting (*10*). In addition, implantation of GES systems may be preceded by the endoscopic placement of a temporary GES system to determine whether this mode of treatment will be beneficial to the patient (*11*). Although the ultimate metric of

[1]Department of Mechanical Engineering, Massachusetts Institute of Technology, Cambridge, MA 02139, USA. [2]Division of Gastroenterology, Hepatology and Endoscopy, Brigham and Women's Hospital, Harvard Medical School, Boston, MA 02115, USA. [3]David H. Koch Institute for Integrative Cancer Research, Massachusetts Institute of Technology, Cambridge, MA 02139, USA. [4]Division of Engineering, New York University Abu Dhabi, Abu Dhabi, UAE. [5]Tandon School of Engineering, New York University, New York, NY 11201, USA. [6]Department of Chemical Engineering, Massachusetts Institute of Technology, Cambridge, MA 02139, USA. [7]Division of Comparative Medicine, Massachusetts Institute of Technology, Cambridge, MA 02139, USA.
†These authors contributed equally to this work.
‡Present address: Memorial Sloan Kettering Cancer Center, New York, NY, USA.
*Corresponding author. Email: cgt20@mit.edu, ctraverso@bwh.harvard.edu (G.T.); kramadi@mit.edu, kbr5930@nyu.edu (K.B.R.)

efficacy is symptom relief in patients, studies have identified that GES can activate vagal afferents and can influence activity of the amygdala, thalamic, and caudate nuclei in the brain (*12*).

Given the higher prevalence of gastroparesis in people with diabetes and the symptomatic benefit of GES, we hypothesized that GES likely exerts a neuromodulatory effect on the gut-brain axis, specifically on the chemoreceptor trigger zone, located within the area postrema in the medulla oblongata, responsible for initiating and coordinating vomiting reflexes. We posited that this neuromodulation is achieved at least in part using direct neuronal excitation via stomach-brain vagal afferent pathways, hormonal modulation, or both. We further posited that similar efficacy could be achieved through mucosal, as opposed to serosal, electrical stimulation through an ingestible system, despite the presence of potentially fouling fluids and solids within the GI tract.

Here, we show that mucosal GES directly induces the release of the orexigenic hormone ghrelin from the gastric mucosa via endoscopic stimulation. We show the replication of this effect using an

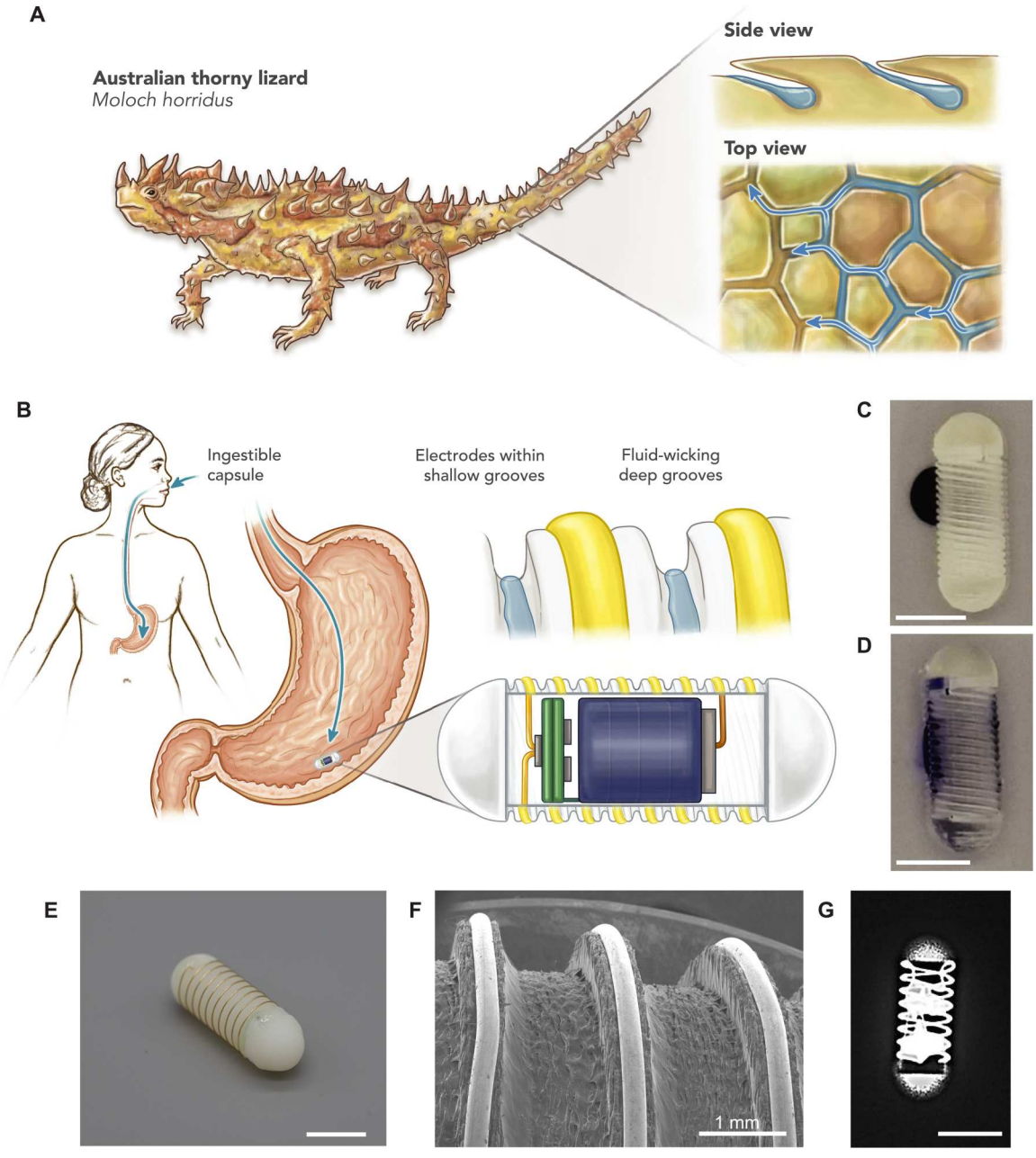

Fig. 1. Overview of bioinspired FLASH design. (**A**) Cartoon showing the role of skin microstructure pattern of *M. horridus* in wicking water. (**B**) Illustration of ingestible FLASH. (**C** and **D**) Effect of nontreated (C) and hydrophilic O_2 plasma–treated (D) grooved capsules on wicking food coloring dye. (**E**) Picture of FLASH. (**F**) Scanning electron microscope image of the FLASH surface showing electrodes and grooves. (**G**) X-ray of assembled FLASH showing internal electronics and circumferential electrodes. Scale bars, 1 cm unless otherwise noted.

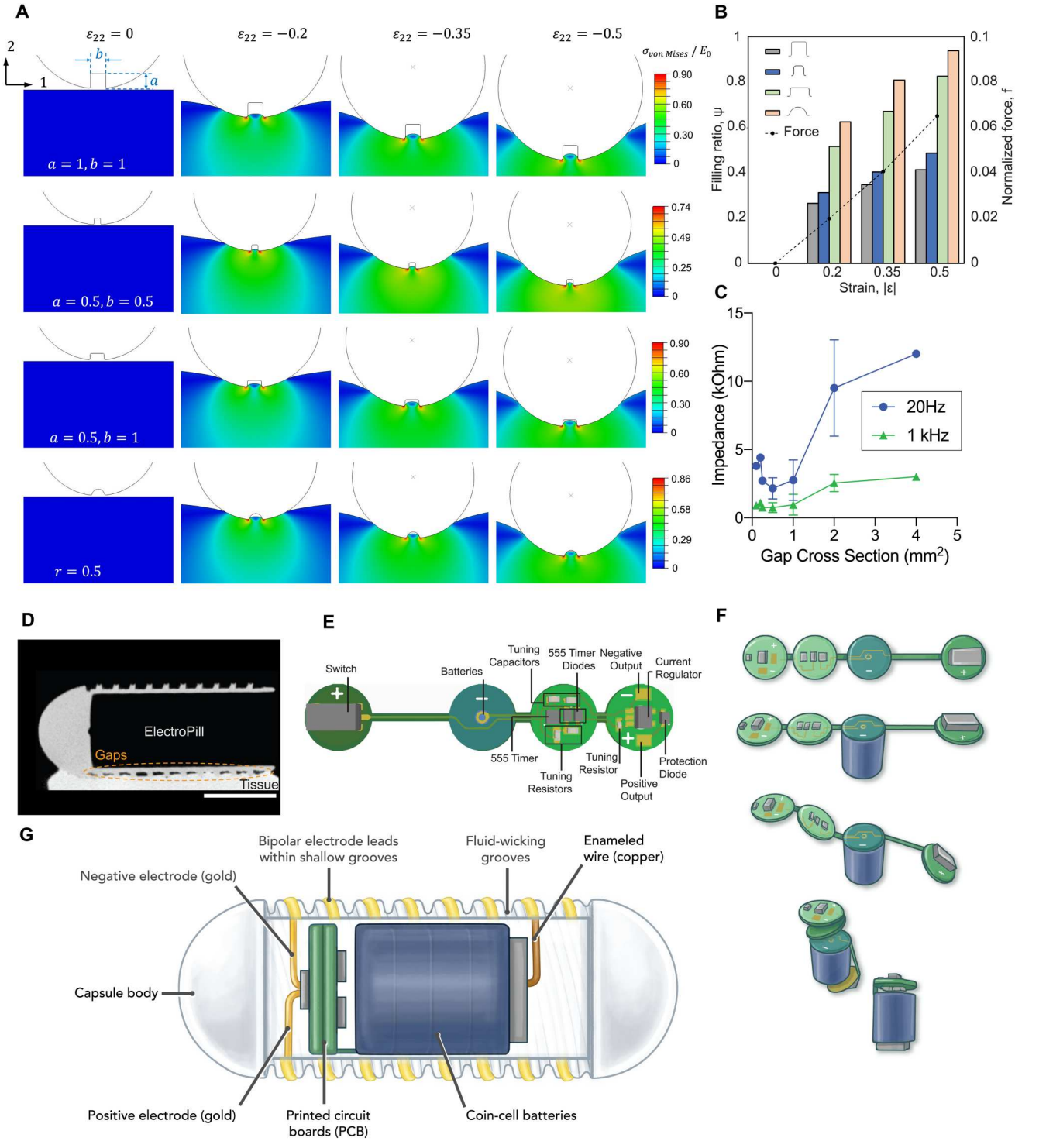

Fig. 2. Optimization of surface grooves and electronics. (**A**) Numerical snapshots obtained from FE simulations showing the effect of a single groove with square (1 mm by 1 mm and 0.5 mm by 0.5 mm), rectangular (0.5 mm by 1 mm), and circular (r = 0.5 mm) shapes on indentation response of the tissue-like rubber at different levels of applied uniaxial strains, ε_{22} = 0, −0.2, −0.35, and −0.5. The counter maps represent the distribution of normalized von Mises stress, $\sigma_{von\ Mises}/E_0$, where E_0 is the initial elastic modulus of the rubber. (**B**) The effect of grooves with different shapes and sizes on filling ratio (ψ; colored columns) and the corresponding normalized indentation force (*f*; dashed black line) as a function of the absolute value of ε_{22}. (**C**) Experimental electrical impedance versus groove cross-sectional area at 20 Hz and 1 kHz. (**D**) CT image of FLASH capsule in contact with porcine gastric mucosa showing gaps in contact created by the grooved pattern. (**E**) Schematic of internal PCB circuits. (**F**) Illustration of flexible PCB folding. (**G**) FLASH cross section showing internal batteries and PCB components as well as external electrodes and grooved surface. Error bars represent SEM.

ingestible electronic capsule. Ghrelin is known to act on central satiety and hunger centers such as the paraventricular hypothalamus, and ghrelin agonists (relamoralin) are under investigation as treatments for nausea and vomiting (*13*). To facilitate the administration of this potential electroceutical through nonsurgical means, we report the development of an ingestible electronic fluid-wicking capsule for active stimulation and hormone modulation (FLASH) that is capable of delivering electrical stimuli to the gastric mucosa. Recognizing the challenges associated with electrical stimulation in the presence of gastric fluid and inspired by the water-wicking skin of *Moloch horridus*, the Australian thorny devil lizard, we developed a fluid-wicking capsule coating, which enables robust electrode-mucosa contact despite the persistent presence of gastric juice (Fig. 1, A to D) (*14*). FLASH consists of internal electronics and batteries that power the electrode, which is wound circumferentially along the device (Fig. 1, E to G). Oral ingestion of FLASH is shown to repeatedly and significantly modulate levels of ghrelin and glucagon-like peptide 1 (GLP-1) in plasma. FLASH is similar in size to the FDA-approved, daily-dosed osmotic-controlled release oral delivery system (OROS) (9 mm by 15 mm). OROS is a nondegradable capsule with obstruction rates of 1 in 29 million (*15*). Beyond ghrelin modulation, FLASH provides a noninvasive platform for ingestible electroceutical interventions for neurohormone modulation. Modification of stimulation parameters and locations could uncover further potential applications in diabetes, obesity, and neuropsychiatric diseases.

RESULTS

The gastric mucosa constantly secretes gastric fluid. We found that the presence of gastric fluid could prevent stable electrode-tissue contact and lead to current shunting, in which electrical stimuli is not adequately transmitted to the tissue. Inspired by the water-wicking skin of the Australian thorny lizard (*M. horridus*), we designed grooved patterns on the surface of FLASH to channel water away from the electrode-tissue interface (Fig. 1, A and B, and fig. S1) (*14*). We observed through endoscopy that devices delivered intragastrically remained partially submerged in gastric fluid in the fasted stomach. On the basis of this, we modeled the behavior of the device in the gastric cavity as that of a partially submerged solid in fluid. To enhance fluid wicking, we generated a hydrophilic surface after O_2 plasma treatment, reducing the contact angle between the pill′s surface and deionized water from 54° to 12° (figs. S2 and S3). Combining grooves with hydrophilic surface treatments enabled the device to sufficiently wick water away from the electrode-tissue interface (Fig. 1, C and D, and figs. S2 to S4).

We optimized groove dimensions analytically by modeling fluid capillary action, computationally using finite element analysis (FEA), and experimentally using benchtop experiments. We balanced practical size limitations, because of capsule dimensions and wall thickness, while maximizing fluid wicking ability. Grooves also needed to remain free of obstruction despite experiencing dynamic GI contractions. We investigated a range of cross-sectional shapes (square, rectangle, and circle). Given a maximum capsule diameter of 9.55 mm and the volume required for internal electronics, we calculated the maximum groove depth to be 0.6 mm. Grooves need to wick fluid to the top of the capsule, a total distance of half of the pill′s circumference (πR), 15 mm. To satisfy these requirements, we selected a rectangular groove cross section with a 1-mm width and a 0.6-mm depth. A rectangular, as opposed to circular or triangular, cross section maximizes the volume of fluid that can be wicked.

We then used nonlinear FEAs to predict the indentation behavior of the capsules with a range of groove shapes and sizes. In Fig. 2A, we show numerical snapshots of capsules with single grooves of various shapes [square (1 m by 1 m, 0.5 mm by 0.5 mm), rectangular (0.1 mm by 1 mm), and circular (r = 0.5 mm)] pushed against a tissue-like soft rubber under uniaxial strain ε_{22}. We monitored the deformation behavior of the rubber by calculating the filling ratio of the grooves (ψ) and the required normalized indentation force (f) as a function of ε_{22} for each groove (Fig. 2B and movies S1 to S5). Square grooves have the lowest ψ, followed by rectangular then circular grooves, whereas f is relatively constant at all levels of ε_{22}. Overall, deeper grooves remain more patent than shallower grooves (Fig. 2, A and B). We opted for rectangular groove designs to balance low ψ while enabling greater wicking efficiency and volume.

Previous studies (*16*) have shown that grooves with rectangular cross sections wick water up to a height, h_{rec}, according to

$$h_{rec} = \frac{\sigma[(2D + W)\cos\theta - W]}{\rho g D W \sin\alpha} \quad (1)$$

where σ is surface tension, D is channel depth, W is channel width, θ is the contact angle, α is the tilt of the column, ρ is fluid density, and g is the gravitational constant.

We conducted in vitro studies to test the effect that various groove dimensions had on electrical impedance across two electrodes placed in contact with a moist tissue phantom. Consistent with our analytical and computational modeling, impedance decreased with groove cross-sectional length up to 0.5 mm^2 (Fig. 2C). Impedance increased with wider grooves because of reduced capillary action. To visualize the fluid-wicking gaps that remain when pills are in contact with tissue, we conducted computed tomography (CT) imaging of grooved capsules placed in contact with ex vivo porcine gastric tissue. CT imaging verified that surface grooves ensure that fluid-wicking gaps remain, even when the fluid is directly in contact with the capsule surface (Fig. 2D and figs. S5 and S6). We further evaluated the indentation behavior of the prototype using FEA (Fig. S7 and movie S6). In these experiments, we modeled the contact of the pill on a flat section of the stomach. We neglected the presence of rugae that are characteristic of stomach given their substantially larger size compared with device grooves.

FLASH contains a flexible printed circuit board (PCB) and two coin cell batteries connected to a wire electrode helically wound about the outside of the entire pill (Fig. 2, E and F, and fig. S8). The PCB uses an astable oscillator circuit, created using a 555 timer, passive capacitors and resistors, and two diodes, to output a square wave voltage sequence (Fig. 2E and fig. S8). A voltage-to-current converter converts this into a square wave current. We used a collapsible PCB to allow these components to fit, along with multiple coin cell batteries, inside the ingestible capsule (Fig. 2, F and G, and fig. S9). To optimize power output and minimize the number of batteries on board, we used a 14-karat gold wire as the electrode, which has low electrical resistivity and is resistant to corrosion, biocompatible, and cost-effective (fig. S10). The wire electrode was helically wrapped along the length of the pill to maximize contact area

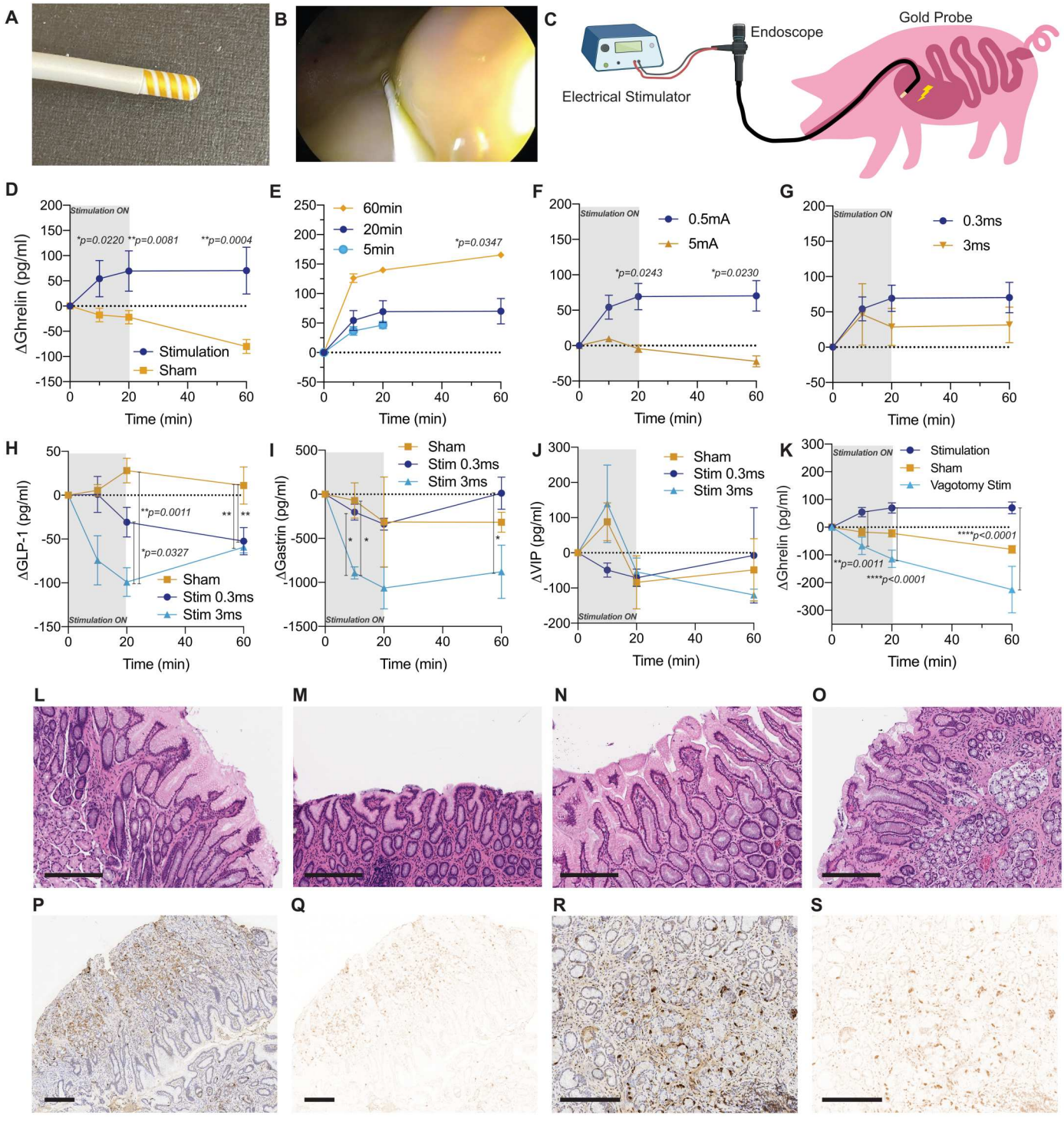

Fig. 3. Hormone modulation through endoscopic GES. (**A**) Bipolar gold probe. (**B**) Endoscope image of gold probe in contact with gastric mucosa. (**C**) Schematic of experimental setup for endoscopic stimulation. (**D** to **G**) Change in plasma ghrelin concentration over time for stimulation versus sham (D); 5, 20, and 60 min of stimulation (E); 0.5- and 5-mA amplitude stimulation (F); and 0.3- and 3-ms PW stimulation (G). (**H** to **J**) Change in plasma concentration of GLP-1 (H), PYY (I), and CCK (J) over 20 minutes of stimulation or sham. (**K**) Change in ghrelin concentration over time after 20 min of stimulation, sham, and stimulation after vagotomy. (**L** to **O**) H&E stains of biopsied gastric mucosa after stimulation at the stimulation site (L and M) and far away from stimulation site (N and O). (**P** to **S**) Ghrelin histological staining of biopsied gastric mucosal tissue near (P and Q) and far away (R and S) from the stimulation site. Scale bars, 200 μm. Error bars represent SEM. *$P < 0.05$ and **$P < 0.005$.

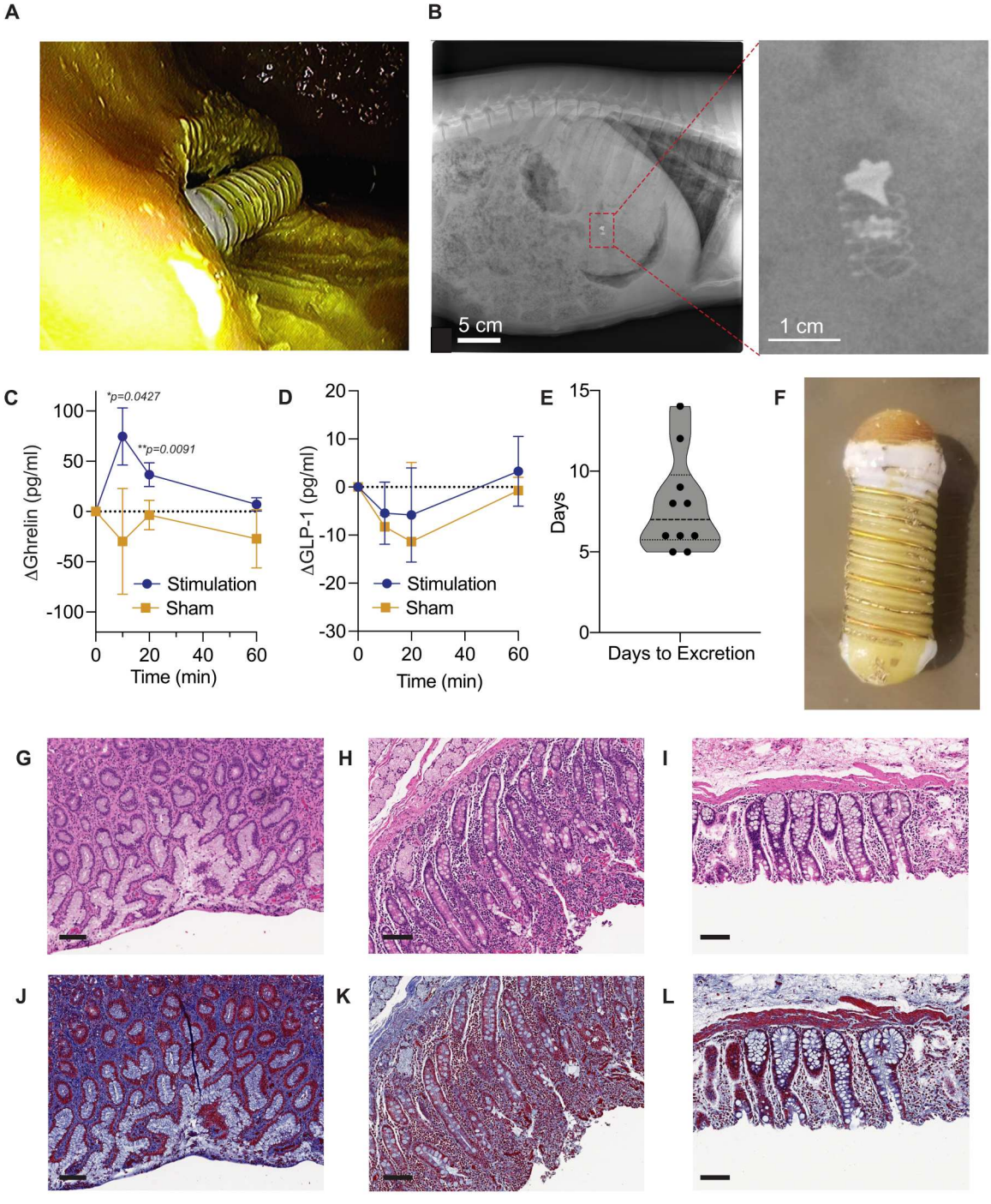

Fig. 4. In vivo administration of FLASH. (**A**) Endoscopic image of FLASH in contact with gastric mucosa. (**B**) Radiograph of swine showing ingested FLASH (inset). (**C** and **D**) Change in plasma (C) ghrelin and (D) GLP-1 concentration over time after delivery of FLASH capsule (stimulation) and nonactive capsule (sham). (**E**) Days to excretion of ingested FLASH. (**F**) Intact FLASH after excretion. (**G** to **L**) H&E (G to I) and Masson's (J to L) stains of stomach (G and J), duodenum (H and K), and colon (I and L) tissue after FLASH passage. Scale bars, 100 μm. Error bars represent SEM. *$P < 0.05$ and **$P < 0.005$.

with tissue. The electrode and the pill surface remained free of fouling after 2 weeks in gastric fluid (fig. S11).

We next sought to understand the neurohormonal effects of GES with a range of parameters: 0.3- to 3-ms pulse width (PW), 14-Hz frequency, 0.5- to 5-mA amplitude, and 5- to 60-min stimulation time. For reference, FDA-approved GES parameters are 0.33 ms, 14 Hz, and 5 mA. We used an endoscopic bipolar gold probe to ensure that the stimulation site and contact pressure would remain the same across studies (Fig. 3, A and B). Gold probes, which are used in gastroenterology for electrocautery, were adapted for our purposes and connected to a benchtop electrical stimulation system (Fig. 3C) (*17*). Gold probes were placed along the greater curvature of the stomach. GES was applied for 20 min consistently and reliably increased plasma ghrelin concentration compared with nonstimulated controls in which probes were placed but stimulation was not turned on (+70.23 pg/ml versus −80.11 pg/ml at 60 min) (Fig. 3D). This effect scaled with the length of the stimulation time. Stimulation for as short as 5 min increased plasma ghrelin concentration (+46.56 pg/ml) relative to sham nonstimulated control (Fig. 3E). The decrease in ghrelin observed in the sham group could be due to effects of inhaled anesthetics and endoscopic intervention, consistent with previously published findings (*18*–*21*).

The level of ghrelin increase was dependent on the electrical stimulation parameters. Stimuli with 0.3-ms PW and 0.5-mA amplitude resulted in the most significant ghrelin changes (Fig. 3, F and G). This is consistent with previous reports comparing the various mechanisms of action of different electrical stimuli (*22*). Neuronal, as opposed to muscular, excitation is best achieved with shorter PWs and smaller amplitudes (*23*). We also investigated the effect of GES on other GI hormones. GES (3-ms PW) consistently decreased plasma GLP-1 levels (−99.1 versus 28.02 pg/ml of sham) (Fig. 3H) and plasma gastrin levels (Fig. 3I). GES did not have a notable effect on peptide YY (PYY) or gastric inhibitory polypeptide (Fig. 3J and fig. S12). Blood cell counts, metabolites, and liver and kidney function enzymes all remained within a normal range after stimulation (fig. S13).

Seeking to elucidate the mechanism of action of ghrelin increase, we repeated stimulation in vagotomized animals. The ghrelin modulation effect of GES was completely abrogated by vagotomy (Fig. 3K). This suggests that the mechanism of controlling plasma ghrelin concentration levels relies on both afferent and efferent stomach-brain circuitry in the vagus nerve. Evaluation of the histology of the stimulation sites by a board-certified pathologist showed no notable morphological changes, bleeding, or tissue damage, supporting the safety of GES over the time spans used here (Fig. 3, L to O, and figs. S14 and S15). Gastric mucosal cells did not show substantially enhanced expression of ghrelin after stimulation (Fig. 3, P to S, and figs. S16 and S17).

Having established a robust effect with an experimentally stable endoscopic stimulation, we next examined whether ghrelin modulation could be replicated using an orally ingested platform. We delivered FLASH to the stomachs of anesthetized animals to the greater curvature of the stomach to replicate the gold probe stimulation (Fig. 4, A and B, and fig. S18). Devices were administered using endoscopy and dropped immediately after passing the esophageal sphincter, settling into the greater curvature of the stomach because of gravity. All animals were fasted overnight before device delivery. In vitro benchtop stimulation studies on agarose phantoms that validated stimulation delivered by both the gold probe and the capsule were identical (fig. S10). To avoid inadvertent stimulation before the device settled in the gastric cavity, we encapsulated the device in a casing to prevent electrode contact with tissue. Isomalt was used as a temporary seal for the protective shell encasing FLASH. Once the isomalt degraded within minutes of contact with moisture in the stomach, the protective shell fell off and deployed the device for stimulation and fluid wicking (figs. S19 and S20). Electrical connections from the batteries, PCB, and electrode wires were soldered with typical non-Pb–based solder wire. The capsule body and internal electronics were sealed with ultraviolet (UV) epoxy.

Similar to endoscopic stimulation, FLASH administration reliably increased plasma ghrelin levels (74.7 versus −29.8 pg/ml of sham). However, no effect was observed on plasma GLP-1 levels (Fig. 4, C and D). We found the impedance of a bipolar electrode applied to gastric mucosa to be on the order of 1 kilohm, assuming optimal contact conditions. On the basis of this, we incorporated a power budget of 90 milliwatt-hour into FLASH to supply electrical stimulation for up to 1 hour. In practice, this would likely be less given that in vivo conditions for tissue-electrode contact are not static.

Pills were well tolerated, retained in the stomach for 1 day, and all passed within 2 weeks of ingestion (Fig. 4E and fig. S21), consistent with prior GI transit times in the porcine model (mean retention time of 7.9 days). Pills supported GI transit and remained intact after excretion (Fig. 4F). Histological examination of GI tissue after pill passage also showed no noticeable trauma, bleeding, or change in morphology as characterized by a board-certified pathologist (Fig. 4, G to L, and fig. S22).

DISCUSSION

It remains challenging to deliver hormone therapies orally because of their poor oral bioavailability. Here, we illustrate how an ingestible electroceutical could potentially modulate systemic hormone levels after oral administration. Crucial to this capability is the rational fluidic design of FLASH to enable fluid wicking away from the stimulation site, enabling robust electrode-tissue contact. Such capabilities could potentially expand the use of electroceuticals. Using a bioinspired surface design together with flexible electronic components, FLASH can deliver specific electrical stimuli to the gastric mucosa. We show that GES exerts its effects in part by modulating ghrelin plasma levels. Although this effect is less than that seen with endoscopic stimulation, nevertheless, reliable increases in plasma ghrelin were observed. The area postrema has been shown to express ghrelin receptors, suggesting a possible mechanism of action by which GES can relieve emetic symptoms in gastroparesis together with previously identified vagal afferent activation (*24*). The effect of GES could potentially be modified by varying both the stimulation site and the stimulation parameters, including PW, amplitude, and time of stimulation. Recent work, for example, has shown that stimulation waves with longer PWs (>3 ms) can induce gastric muscle contraction (*25*). However, such stimulation requires considerable power to sustain, necessitating power-harvesting techniques or wireless powering strategies for ingestible devices (*26*, *27*).

We also report the unexpected finding that, although ghrelin is a hormone released by gastric cells, GES only induces an increase in

plasma ghrelin levels while the vagus nerve is intact. This suggests that GES activates a vagal reflex that then regulates ghrelin production. This is consistent with findings that GES activates vagal afferents that centrally mediate symptoms of nausea and vomiting (*12*). An alternate explanation could be that GES leads to a decrease in the transport of acylated ghrelin across the blood-brain barrier into the brain (*28*). Last, it is possible that local spreading of current along the mucosa directly stimulates P/D1 cells and that vagotomy is simply suppressing the food deprivation–mediated rise in ghrelin as it is known to do (*29*). We focused our analysis in vagotomized animals on ghrelin as the primary hormone of interest. Although these findings are consistent with some studies suggesting that GES effects may be centrally mediated, future research elucidating the anatomic pathways of this effect could be helpful in developing more targeted electroceutical therapies for neurohormonal modulation (*30*).

FLASH is designed to be ingested, deliver stimulation for at least 20 min, and thereafter pass through the GI tract and be excreted. Given that the onboard batteries supplied energy for ~20 min of stimulation and that pills were retained in the stomach for 1 day, it is unlikely that any stimuli were delivered to the distal GI tract. Distal GI stimulation could, however, be leveraged to modulate other neurohormonal and immune pathways. Duodenal electrical stimulation has been shown to reduce food intake, elevate plasma GLP-1, and improve glucose tolerance (*31*, *32*). Colonic electrical stimulation can potentially reduce inflammation and accelerate colonic transit time (*33*, *34*). Future work could explore how mucosally delivered stimulation might similarly affect neural and hormonal circuits in these regions.

Surface treatment of FLASH is an essential design component. We leveraged O_2 plasma treatment as a facile method to readily achieve high hydrophilicity sufficient for micro- and milliscale fluid wicking that remains on the order of hours. However, plastic surfaces treated solely with O_2 plasma treatment will result in transient hydrophilicity. There also exist alternate approaches to induce permanent hydrophilicity on surfaces (*35*–*37*). Permanent hydrophilic surfaces are commonly used in a range of commercial products where a consistent fluid-wicking behavior is needed, including antifog glasses, swabs for medical tests, syringes and capillaries, respirators, and perspiration-wicking fabric. Various protective shells and coatings can also be used to prevent a hydrophilic surface from saturating prematurely. FLASH uses a capsule shell held together with isomalt sugar, which degrades within minutes, sufficient to ensure that the device reaches the stimulation target along the greater curvature of the stomach. If small intestinal stimulation was desired, then a similar shell could be used that leverages an enteric polymer coating that will not dissolve in the low pH of the stomach but will dissolve in the higher-pH small intestine to release the capsule from its protective shell.

Materials will need to be cost-effective and biocompatible to justify the use of electronic pills that can be regularly administered similarly to oral pharmacotherapies. FLASH uses 28-mAh silver oxide batteries (728-1111-ND from Seiko Instruments) with dimensions of 6.8 mm by 2.6 mm. These batteries are used in FDA-approved ingestible devices such as the PillCam and cost about $1 per battery. The PCB components are aligned with common electronic systems and materials used in FDA-approved ingestible systems. FLASH does not have any wireless communication or microprocessors and uses a fairly simple circuit that is cost-effective, especially at scale. Surface electrodes are gold wires (30 gauge, 14 karat). Gold is regarded as a highly biocompatible metal, and the cost of this wire is about $2 to $4 per device. The capsule material itself leverages stereolithography (SLA) three-dimensional (3D) printing of simulated polypropylene materials. This allows for reliable fabrication of microscale surface features, which can be done affordably with biocompatible SLA resins. If faster fabrication rates are needed for large device quantities, then computer numerical control (CNC) machining of polypropylene can be used instead with similar overall costs. Further translation aims to also explore manufacturing and scaling up of these devices to be compliant with ISO 10993 (Biological evaluation of medical devices) and ISO 14708 (Active implantable medical devices) with respect to transiting ingestible medical devices.

Devices incorporating gastric retention techniques could be designed for repeated stimulation of gastric mucosa over multiple days or weeks (*38*). However, such devices would have higher power requirements and would need additional features, such as mucosal adhesives, to ensure adequate electrode-mucosa contact over time (*39*–*41*). The fluid-wicking mechanism developed here could be used for a number of other applications in ingested systems, including sampling of luminal fluids for diagnosis of metabolic or functional GI disorders. The optimal surface treatment of the device depends on the extent to which the device remains submerged within gastric fluid. Our studies illustrate that hydrophilic surface treatment is sufficient to enable device functionality even when it is partially submerged in fluid. However, a completely submerged device may benefit from a hydrophobic, rather than hydrophilic, surface to reduce fouling of the electrode-tissue interface, especially during the initial delivery phase before coming into contact with gastric mucosa. The weight and the effective density of the pill also need to be designed to ensure that the pill does not float in the presence of fluids. The capillary attraction force between the wetted pill and the gastric mucosa could also be optimized to overcome lubrication forces that may prevent a stable device-tissue contact. In our case, we estimate that capillary attraction forces are an order of magnitude less than the weight of FLASH (2.5 versus 25 mN). However, such design choices need to balance the various forces acting on ingested devices, including gravity, gastric contractions, and device-mucosa interactions. This could be incorporated into other ingestible devices that have been reported for similar indications (*42*). Other parameters that may affect device-tissue interaction are irregularities in the tissue surface, such as gastric rugae and intestinal villi. Swine are the ideal preclinical model for GI disorders because they have similar anatomy and physiology to humans (*43*). Our experiments in swine suggest that gastric rugae do not interfere with FLASH functionality.

FLASH represents an ingestible electroceutical that could be used to modulate hormone levels, potentially influencing hunger and satiety circuitry in the brain and feeding behavior. This could be relevant as symptomatic therapy of chronic nausea and vomiting syndromes, eating disorders, and cachexia. A primary goal of therapy in patients with severe anorexia nervosa, for example, is weight regain. The extent and speed of weight regain can predict outcomes and prognosis. Hunger-promoting therapies could enhance this regain. Ghrelin has been previously administered to patients as an intravenous infusion or bolus for indications including anorexia nervosa, cachexia, cancer, and gastroparesis (*44*). In one study, a 3.5-fold increase in plasma ghrelin enhanced food

intake by 40% in cancer patients with impaired appetite (*45*). In another, a threefold increase in plasma ghrelin decreased gastric retention (*46*). Mucosal GES in our studies here similarly led to a two- to fivefold increase in plasma ghrelin levels, supporting the clinical relevance of our approach. Furthermore, orally administered FLASH would avoid the need for injections and removal of clothes for administration.

The size and architecture of FLASH are similar to FDA-approved ingestible capsule endoscopy (PillCam) systems and OROS capsules, and FLASH delivers stimulation identical to the FDA-approved GES system, supporting clinical utility (*15*, *47*). Devices on the size scale of the OROS system (9 mm by 15 mm) have shown very low obstruction incidence rates of only 1 in more than 76 million tablets administered (*15*). In its current embodiment, FLASH would be used in fasting patients. Further evaluation of FLASH's functionality in the presence of food and other common states of the gastric environment will be critical to informing its application space, especially in anticipation of clinical trials. FLASH could also be modified to enable chronic stimulation that would include gastric retention mechanisms, wireless communication, and wireless power transfer for sustained and controlled stimulation. Although we have validated the functionality of FLASH in empty, fasted stomachs, future prototypes could incorporate robotic or active elements to assist with navigation and functionality in stomachs with ingested fluids and solids (*48*).

Future work could also dissect physiological mechanisms and specific neuronal circuits affected by electrical stimulation. In-depth mechanistic studies on vagal recordings and GLP-1 modulation could offer insights to explore other potential disease indications that GES might be applicable to. Delivery of electrical stimuli through ingested platforms could enable a new type of therapy combining the best of current pharmacologic, surgical, and electroceutical approaches. Future ingestible electroceutical systems could be designed and customized for specific applications beyond acute, short-term gastric stimulation. FLASH is orally administered, similar to most commonly used medications and unlike GES systems. Unlike medications, it specifically targets gastric neurohormonal circuits to modulate hormone levels in the blood. Such hormone modulation can usually only be accomplished through needle injections. FLASH acts on the gastric mucosa and is then safely excreted, avoiding the risks of invasive procedures and GES implantation (*3*). FLASH is a platform to inform ingestible electroceutical development that could potentially be used for certain GI, neuropsychiatric, and metabolic disorders.

MATERIALS AND METHODS

Numerical simulations

The simulations were carried out using the commercial Finite Element (FE) package Abaqus 2017 (SIMULIA, Providence, RI). The Abaqus/Standard solver was used for the simulations. We constructed 2D FE models of the rigid capsules with various groove patterns and a soft elastomeric matrix (silicone-based rubber as a tissue-like material) to investigate the effects of groove shapes and sizes on the deformation behavior of the tissue under compression.

We used four-node bilinear plane stress quadrilateral elements with reduced integration and hourglass control (Abaqus element type CPS4R) to construct the FE models of the soft elastomeric matrix. The material behavior of the elastomer was captured using a nearly incompressible Neo-Hookean hyperelastic model (Poisson's ratio of ν_0 = 0.499 and initial elastic modulus of E_0 = 80 MPa) with directly imported uniaxial compression test data. Two-dimensional plane stress two-node linear discrete rigid elements (Abaqus element type R2D2) were used to build the models of capsules with four different groove patterns. Square-shaped (1 mm by 1 mm and 0.5 mm by 0.5 mm), rectangular-shaped (1 mm by 0.5 mm), and circular-shaped (r = 0.5 mm) grooves were considered. A simplified contact law (surface-to-surface type interaction) was assigned to the surfaces of elastomer and capsule models with a penalty friction coefficient of 0.3 for tangential behavior and "hard" contact for normal behavior. The rigid capsules were initially positioned slightly above the tissue surface. We performed static analysis to examine the nonlinear compression behavior of the tissue by lowering the capsules down to 50% of the capsule diameter. We monitored the reaction forces of the capsules as a function of applied displacement in the normal direction for the aforementioned groove patterns. The filling ratios, ψ, were then computed by $\psi = 1 - A_{\text{Void}}/A_{\text{Groove}}$, where A_{Void} and A_{Groove} are the areas of free space inside the groove at different levels of deformation and grooves, respectively, measured via image analysis of the obtained numerical snapshots. The reaction forces were normalized as $f = F_{22}/E_0A$, where F_{22} is the reaction force in 22 directions as defined in Fig. 2, E_0 is the initial elastic modulus of the elastomeric rubber, and A is the cross-sectional area of the capsule.

Contact angle measurements

Planar samples without any surface features were fabricated via 3D printing of RGD450 resin using a Stratasys. These samples underwent various surface treatments (no-treatment control, 1-min 50-W O_2, 5-min 50-W O_2, and 5-min 100-W O_2). Then, on separate samples, 20 μl of deionized water and 20 μl of real gastric fluid were placed on the sample. Side-view images were captured, and the contact angle was measured using ImageJ software.

Fluid wicking

Three capsules were fabricated via 3D printing of clear resin using a Formlabs printer. One capsule had a smooth surface, and the remaining two had the optimized grooves on the surface (1-mm wide by 0.6-mm deep). One grooved capsule remained untreated as a control. The smooth capsule and remaining grooved capsule were treated in O_2 plasma (5 min, 100 W; AutoGlow by Glow Research). These capsules were then placed into separate petri dishes, and a video was recorded as 200 μl of a methylene blue solution were dispensed under each sample to evaluate the wicking functionality.

Fluid wicking analysis

The capsules were fabricated from a simulated polypropylene material (RGD450 by Stratasys) that is inherently hydrophobic (contact angle of ~100°). Fluid wicking in a horizontal rectangular three-walled channel can be described by the following equation (*16*):

$$h_{\text{rec}} = \frac{\sigma[(2D + W)\cos\theta - W]}{\rho g D W} \quad (2)$$

where σ is surface tension, D is the channel diameter, W is the channel height, θ is the contact angle, ρ is fluid density, and g is the gravitational constant.

The contact angle plays a critical role in the ability of a microgroove to wick fluid. To reduce contact angle and improve hydrophilicity, we applied plasma treatment to the capsule surface. This improved the capsule's wicking ability.

We estimated the Reynold's number within our capsule grooves to justify assumptions about the flow profile in microgrooves. For a rectangular channel with an open top, the Reynold's number is defined as

$$Re = \frac{\rho V D_h}{\mu} \quad (3)$$

where ρ is the fluid density; V is the fluid velocity; D_h is the hydraulic diameter given by $\frac{4*A_c}{l}$, where A_c is the cross-sectional area and l is the wetted perimeter; and μ is the dynamic viscosity of the fluid.

The density of water is about 1 g/cm^3, and the hydraulic diameter of the grooves is 1.01 mm (1-mm wide by 0.6-mm deep). Per our dye wicking experiment (fig. S4), the velocity is estimated to travel half of the capsule circumference (12.7 mm; fig. S24) in about 2 s, resulting in a velocity of 0.0064 m/s. The dynamic viscosity of water is 8.9×10^{-4} N*s/m^2. This results in a Reynold's number of 7.8 for the dye-wicking case with the plasma-treated capsule. This is consistent with micro- and milliscale fluidics given the very small dimensions. Given the capsule outer diameter (within the groove base) of 8.1 mm, the required wicking height can be estimated to be about half of the capsule circumference, which is approximately 12.7 mm. Measured contact angles can be used to determine wicking heights after various plasma treatments.

Capillary wetting force analysis

We modeled the attractive force between the device and mucosa as the capillary force that attracts a partially wetted cylinder to a flat surface using the typical radius of curvature of the meniscus near the pill, R, and the surface tension, γ, of the fluid-air interface. This creates a Laplace pressure of γ/R. For the case where the meniscus begins halfway up the pill, the capillary force, F_{cap}, can be calculated as

$$F_{cap} = \frac{LD\gamma}{R} \quad (4)$$

where L is the length of the cylinder and D is the cylinder's diameter. If we assume that L = 18 mm, D = 9 mm, γ = 72.8 mN/m, and R = 4.7 mm (fig. S23), then F_{cap} = 2.5 mN.

In vitro impedance testing

A range of planar samples were fabricated via 3D printing in RGD450 resin using a Stratasys printer. Sample surface features included rectangular grooves and triangular grooves. Rectangular groove dimensions ranged from 0.1 to 2 mm in both width and depth. Triangular grooves had sloped surfaces at 30°, 45°, and 60°. For the rectangular and triangular samples, two copper wires were epoxied to the patterned sides. For the cylindrical posts, gold films were sputtered onto the top of the posts. These samples were then connected to the terminals of an LCR meter, the sample was placed pattern-side down onto an agarose [2% (w/v) in phosphate-buffered saline (PBS)] phantom, and the impedance was measured. This measurement was taken for each sample in both dry (no PBS dispensed on surface) and wet (100 μl of PBS dispensed on surface before each measurement) scenarios.

FLASH fabrication

Capsule bodies and caps were designed using CAD software (SolidWorks, Waltham, MA) and printed in RGD450 resin on a Stratasys printer at a maximum layer resolution to ensure appropriate groove dimensions for both the wicking (1 mm) and electrode (hundreds of micrometers) grooves. Battery stacks were assembled using conductive silver epoxy to stack two 1.5-V silver oxide batteries in series with a short length of enameled copper wire running from both the positive and the negative terminals of the battery stack. The gold electrode wires were soldered to the output side of the cylindrical PCB. Immediately before assembly, the capsule bodies were placed in an O_2 plasma cleaner (AutoGlow from Glow Research) for 5 min at 100 W to make the capsule surface hydrophilic. After that, the gold wires attached to the PCB were fed through the capsule and out of the holes at the bottom. The two enameled wires on the battery stack were then soldered on to their respective terminals on the battery side of the cylindrical PCB. All wire connections (electrode-PCB, copper-PCB, and copper-battery stack) were secured with a drop of UV cure epoxy (Loctite 4305). All electronics (PCB and batteries) were then fed into the capsule, the wire electrode was wound around the capsule, and everything was secured using UV cure epoxy (Loctite 4305). Capsule functionality was evaluated using an oscilloscope connected to the two concentric capsule electrodes. To encapsulate FLASH, a two-part shell was designed using SolidWorks and printed VeroClear (RGD810) resin using a Stratasys printer. Isomalt was heated with a soldering iron and melted onto the casing to create a seal.

FLASH electronics

The PCB was designed to contain three separate sections. The first is a method of turning the device on and off, which is accomplished with a simple switch. The second section is an astable oscillator created using a 555 timer, passive capacitors and resistors, and two diodes to allow us to more precisely control the duty cycle. This section creates a voltage square wave of the desired duty cycle. The third section is a PSSI2021SAY115 constant current regulator that converts the voltage square wave into a constant current square wave. The flexible circuit boards were ordered and populated through Journey Circuits Inc. (Schaumburg, IL). The FLASH was assembled using 8331S-15G silver conductive epoxy to attach the batteries to the positive and negative input pads and soldering wires to the positive and negative output pads.

Capsule electron microscopy

Scanning electron micrograph pictures of FLASH were taken using the high-vacuum secondary electron detector from the Hitachi FlexSEM TM-1000 II. Low-voltage imaging (2 kV) was not only used in substitution of a conductive coating but also provided high surface detail. The scanning electron microscopy images were captured using frame integration to average out surface charging artifacts. To overcome specimen topography, long working distances (13.5 to 19.0 mm) were used to provide greater depth of field. The built-in ruler was used to measure the dimensions of the electrode and capsule grooves.

Ex vivo CT

Swine tissue for ex vivo evaluation was acquired from the Blood Farm Slaughterhouse (West Groton, USA). Swine were euthanized, and fresh gastric tissue was procured and stored on ice. Slabs of

gastric tissue (2 cm by 2 cm) including both mucosa and serosa were cut and placed into plastic cubes (3 cm by 3 cm). Pill prototypes were placed on the gastric tissue and transferred to a CT system for imaging. A Bruker SkyScan 1276 was used to acquire a series of images with a rotation step size of 1° over 360° with continuous gantry rotation. Images were acquired with x-ray tube settings of 55 kVp, 200 mA, and an exposure time of 200 ms with a 0.25-mm aluminum beam filter. Detector binning (4 by 4) was used for an isotropic resolution of 40.16 μm. Image reconstruction was performed using the Bruker NRecon software.

In vivo endoscopic stimulation

All animal experiments were performed in accordance with protocols approved by the Committee on Animal Care at the Massachusetts Institute of Technology. To assess the effect of mucosal gastric stimulation, we delivered electrical stimulation in a large animal model (30- to 75-kg Yorkshire swine; Cummings School of Veterinary Medicine at Tufts University, Grafton, MA). This model was chosen because its gastric anatomy is similar to that of humans and is frequently used to evaluate devices in the GI tract (*49*, *50*). Animals were fed daily in the morning and in the evening with a diet consisting of pellets (laboratory mini-pig grower diet, 5081), in addition to a midday snack consisting of various fruits and vegetables. Sample sizes were chosen on the basis of preliminary experiments and our prior work with ingestible devices, so as to provide sufficient power for statistical comparison (where appropriate).

Animals were fasted overnight before procedures to ensure safe anesthesia and to avoid aspiration. Pigs were sedated with Telazol (5 mg/kg; tiletamine/zolazepam) and xylazine (2 mg/kg) or cexmedetomidine (0.03 mg/kg) and midazolam (0.25 mg/kg), intubated, and maintained on 1 to 3% isoflurane in oxygen. Their heart rate, respiratory rate, end tidal CO_2, SpO_2, and temperature were monitored while anesthetized. An endoscopic overtube (US Endoscopy) was placed in the gastric cavity under endoscopic visual guidance during esophageal intubation.

A bipolar gold probe (Boston Scientific) was introduced through the endoscopic overtube. Intragastric endoscopy videography was used for image capture of gold probe placement. The probe tip was placed snugly into gastric mucosal lining within 5 cm of the pylorus, and the stomach deflated to ensure optimal contact. The probe was connected to an external electrical stimulation system (A-M Systems model 2100). Stimulation was turned on for 5, 20, or 60 min. Blood was collected at 0, 10, 20, and 60 min after stimulation was turned on via venous catheter. Blood was collected into EDTA tubes (5 ml per tube) for hormone analyses and complete blood count. Blood was collected into serum tubes (5 ml per tube) for chemical chemistry tests. After the final blood draw, gastric mucosa biopsies were taken via endoscopy and placed in 10% formalin.

In vagotomy experiments, a bilateral vagotomy was performed via surgical cutdown on the neck and access to the carotid sheath and isolation of the vagus nerve. Endoscopy was performed immediately afterward, and stimulation began within 5 min. Animals were fasted similarly to other endoscopy procedures.

FLASH administration, stimulation, and passage

FLASH was introduced into the gastric cavity endoscopically through an esophageal overtube and visualized via the endoscope camera. All animal procedures, including fasting and anesthesia parameters, replicated those performed in the endoscopic stimulation with the gold probe. Blood was collected at 0, 10, 20, and 60 min after device administration. Animals were then imaged using radiography at 2- to 4-day intervals thereafter to determine the residency time of the devices and to look for any abnormalities such as signs of obstruction. Radiographs were taken until devices passed. Excreted devices were retrieved from cage bedding. To determine the effect of device passage on GI mucosa, some animals were euthanized 1 week after device administration using sodium pentobarbital (100 mg/kg, intravenously) after sedation, and tissue samples of the GI tract were collected and placed in 10% formalin. Throughout passage studies, animals were evaluated clinically for normal feeding and stooling patterns. There was no evidence of GI morbidities assessed by endoscopy and radiography or any changes in feeding or stooling patterns.

Hormone analysis

Blood was collected from animals via venous catheter into EDTA tubes (5 ml per tube). For ghrelin analysis, EDTA tubes were prefilled with 4-(hydroxymercuri)benzoic acid sodium (10 mM, 300 μl). Blood was centrifuged at 3000 rpm for 10 min. Plasma was carefully removed and distributed into 500-ml aliquots. HCl (10%, 1 N) was added to each vial before storage at −80°C. Blood collected for other hormone analysis was prefilled with Pefabloc, a cocktail of protease inhibitors (Roche). Hormone analysis was conducted using a number of enzyme-linked immunosorbent assays (ELISAs): ghrelin acylated porcine ELISA (BioVendor R&D, Asheville, NC), GLP-1 porcine ELISA (MyBioSource), gastrin porcine ELISA (Biomatik, Wilmington, DE), PYY porcine ELISA (MyBioSource), and VIP porcine ELISA (LSBio, Seattle, WA).

Histology

Isolated gastric biopsies and GI tissue were placed into a solution of 10% neutral buffered formalin (VWR) for 72 hours and then transferred into a 70% ethanol solution. After tissue fixation, tissues were embedded in paraffin and sliced into 5-μm-thick sections. Sections were placed on glass slides and stained according to one of two techniques: Half the slides were stained with hematoxylin and eosin (H&E) to examine tissue morphology, and the other half were stained for ghrelin [primary: goat anti-ghrelin antibody ab104307 (Abcam, Cambridge, MA; 2 μg/ml); secondary: donkey anti-goat IgG H&L (ab205723)]. These samples were analyzed by a board-certified pathologist.

Statistics

Results across groups were compared using unpaired *t* test or analysis of variance (ANOVA). All error bars represent SEM, and the sample size is shown in table S2. Figure captions contain details on *P* values reported for each figure.

Supplementary Materials

This PDF file includes:
Figs. S1 to S24
Tables S1 and S2

Other Supplementary Material for this manuscript includes the following:
Movies S1 to S5
MDAR Reproducibility Checklist

View/request a protocol for this paper from *Bio-protocol*.

REFERENCES AND NOTES

1. A. Gaman, B. Kuo, Neuromodulatory processes of the brain-gut axis. *Neuromodulation* **11**, 249–259 (2008).
2. J. M. Wo, T. V. Nowak, S. Waseem, M. P. Ward, Gastric electrical stimulation for gastroparesis and chronic unexplained nausea and vomiting. *Curr. Treat Options Gastroenterol.* **14**, 386–400 (2016).
3. S. C. Payne, J. B. Furness, M. J. Stebbing, Bioelectric neuromodulation for gastrointestinal disorders: Effectiveness and mechanisms. *Nat. Rev. Gastroenterol. Hepatol.* **16**, 89–105 (2019).
4. S. L. Prescott, S. D. Liberles, Internal senses of the vagus nerve. *Neuron* **110**, 579–599 (2022).
5. Food and Drug Administration, Re: H990014 Gastric Electrical Stimulation (GES) System with Itrel Model 7425 Implantable Pulse Generator, Model 4300 Lead, Model 7432 Physician Programmer, and Model 7457 MemoryMod Software Cartridge (2000); www.accessdata.fda.gov/cdrh_docs/pdf/H990014A.pdf.
6. S. P. Harrell, J. L. Studts, G. W. Dryden, J. Eversmann, L. Cai, J. M. Wo, A novel classification scheme for gastroparesis based on predominant-symptom presentation. *J. Clin. Gastroenterol.* **42**, 455–459 (2008).
7. A. E. Bharucha, Y. Kudva, A. Basu, M. Camilleri, P. A. Low, A. Vella, A. R. Zinsmeister, Relationship between glycemic control and gastric emptying in poorly controlled type 2 diabetes. *Clin. Gastroenterol. Hepatol.* **13**, 466–476.e1 (2015).
8. R. J. Mason, J. Lipham, G. Eckerling, A. Schwartz, T. R. DeMeester, Gastric electrical stimulation. *Arch. Surg.* **140**, 841–846 (2005).
9. T. L. Abell, G. Yamada, R. W. McCallum, M. L. Van Natta, J. Tonascia, H. P. Parkman, K. L. Koch, I. Sarosiek, G. Farrugia, M. Grover, W. Hasler, L. Nguyen, W. Snape, B. Kuo, R. Shulman, F. A. Hamilton, P. J. Pasricha, Effectiveness of gastric electrical stimulation in gastroparesis: Results from a large prospectively collected database of national gastroparesis registries. *Neurogastroenterol. Motil.* **31**, e13714 (2019).
10. P. Ducrotte, B. Coffin, B. Bonaz, S. Fontaine, S. Bruley Des Varannes, F. Zerbib, R. Caiazzo, J. C. Grimaud, F. Mion, S. Hadjadj, P. E. Valensi, L. Vuitton, G. Charpentier, A. Ropert, R. Altwegg, P. Pouderoux, E. Dorval, M. Dapoigny, H. Duboc, P. Y. Benhamou, A. Schmidt, N. Donnadieu, G. Gourcerol, B. Guerci, A. M. Leroi, G. Prevost, E. Huet, M. Robert, E. Disse, Q. Denost, B. Castel, D. Calabrese, S. Borot, P. Mathieu, E. Letessier, F. Vavasseur, F. Reche, N. Mathieu, F. Borie, A. Penfornis, H. Hanaire, N. Jeandidier, P. Fontaine, Gastric electrical stimulation reduces refractory vomiting in a randomized crossover trial. *Gastroenterology* **158**, 506–514.e2 (2020).
11. S. R. Daram, S.-J. Tang, T. L. Abell, Temporary gastric electrical stimulation for gastroparesis: Endoscopic placement of electrodes (ENDOstim). *Surg. Endosc.* **25**, 3444–3445 (2011).
12. R. W. McCallum, R. W. Dusing, I. Sarosiek, J. Cocjin, J. Forster, Z. Lin, Mechanisms of symptomatic improvement after gastric electrical stimulation in gastroparetic patients. *Neurogastroenterol. Motil.* **22**, 167–167 (2010).
13. A. Lembo, M. Camilleri, R. M. Callum, R. Sastre, C. Breton, S. Spence, J. White, M. Currie, K. Gottesdiener, E. Stoner; RM-131-004 Trial Group, Relamorelin reduces vomiting frequency and severity and accelerates gastric emptying in adults with diabetic gastroparesis. *Gastroenterology* **151**, 87–96.e6 (2016).
14. W. C. Sherbrooke, A. J. Scardino, R. de Nys, L. Schwarzkopf, Functional morphology of scale hinges used to transport water: Convergent drinking adaptations in desert lizards (Moloch horridus and Phrynosoma cornutum). *Zoomorphology* **126**, 89–102 (2007).
15. D. M. Bass, M. Prevo, D. S. Waxman, Gastrointestinal safety of an extended-release, non-deformable, oral dosage form (OROS: A retrospective study). *Drug Saf.* **25**, 1021–1033 (2002).
16. G. Bamorovat Abadi, M. Bahrami, A general form of capillary rise equation in microgrooves. *Sci. Rep.* **10**, 19709 (2020).
17. ASGE technology committee, M. A. Parsi, A. R. Schulman, H. R. Aslanian, M. S. Bhutani, K. Krishnan, D. R. Lichtenstein, J. Melson, U. Navaneethan, R. Pannala, A. Sethi, G. Trikudanathan, A. J. Trindade, R. R. Watson, J. T. Maple; ASGE Technology Committee Chair, Devices for endoscopic hemostasis of nonvariceal GI bleeding (with videos). *VideoGIE* **4**, 285–299 (2019).
18. E. Besnier, A. Perdrix, A. Gillibert, J. Selim, B. Froëmer, A. Ghemired, B. Berby, N. Rives, B. Dureuil, T. Clavier, V. Compère, Postoperative hunger after outpatient surgery in patients anesthetized with propofol vs sevoflurane: A randomized-controlled trial. *Can. J. Anesth.* **67**, 550–559 (2020).
19. A. Stengel, M. Goebel-Stengel, L. Wang, A. Shaikh, N. W. Lambrecht, J. Rivier, Y. Taché, Abdominal surgery inhibits circulating acyl ghrelin and ghrelin-O-acyltransferase levels in rats: Role of the somatostatin receptor subtype 2. *Am. J. Physiol. Gastrointest. Liver Physiol.* **301**, G239–G248 (2011).
20. M. Nematy, A. E. Brynes, P. I. Hornick, M. Patterson, M. A. Ghatei, S. R. Bloom, S. J. Brett, G. S. Frost, Postprandial ghrelin suppression is exaggerated following major surgery; implications for nutritional recovery. *Nutr.Metab.* **4**, 20 (2007).
21. M. Wagner, P. Probst, M. Haselbeck-Köbler, J. M. Brandenburg, E. Kalkum, D. Störzinger, J. Kessler, J. J. Simon, H. C. Friederich, M. Angelescu, A. T. Billeter, T. Hackert, B. P. Müller-Stich, M. W. Büchler, The problem of appetite loss after major abdominal surgery: A systematic review. *Ann. Surg.* **276**, 256–269 (2022).
22. K. B. Ramadi, S. S. Srinivasan, G. Traverso, Electroceuticals in the gastrointestinal tract. *Trends Pharmacol. Sci.* **41**, 960–976 (2020).
23. Z. Lin, J. D. Z. Chen, Developments in gastrointestinal electrical stimulation. *Crit. Rev. Biomed. Eng.* **45**, 263–301 (2017).
24. A. Cabral, M. P. Cornejo, G. Fernandez, P. N. de Francesco, G. Garcia-Romero, M. Uriarte, J. M. Zigman, E. Portiansky, M. Reynaldo, M. Perello, Circulating ghrelin acts on GABA neurons of the area postrema and mediates gastric emptying in male mice. *Endocrinology* **158**, 1436–1449 (2017).
25. A. Abramson, D. Dellal, Y. L. Kong, J. Zhou, Y. Gao, J. Collins, S. Tamang, J. Wainer, R. M. Manus, A. Hayward, M. R. Frederiksen, J. J. Water, B. Jensen, N. Roxhed, R. Langer, G. Traverso, Ingestible transiently anchoring electronics for microstimulation and conductive signaling. *Sci. Adv.* **6**, eaaz0127 (2020).
26. P. Nadeau, D. El-Damak, D. Glettig, Y. L. Kong, S. Mo, C. Cleveland, L. Booth, N. Roxhed, R. Langer, A. P. Chandrakasan, G. Traverso, Prolonged energy harvesting for ingestible devices. *Nat. Biomed. Eng.* **1**, 0022 (2017).
27. R. Wang, Z. Abukhalaf, A. Javan-Khoshkholgh, T. H. H. Wang, S. Sathar, P. du, T. R. Angeli, L. K. Cheng, G. O'Grady, N. Paskaranandavadivel, A. Farajidavar, A miniature configurable wireless system for recording gastric electrophysiological activity and delivering high-energy electrical stimulation. *IEEE J. Emerg. Sel. Top. Circ. Syst.* **8**, 221–229 (2018).
28. E. M. Rhea, T. S. Salameh, S. Gray, J. Niu, W. A. Banks, J. Tong, Ghrelin transport across the blood-brain barrier can occur independently of the growth hormone secretagogue receptor. *Mol. Metab.* **18**, 88–96 (2018).
29. D. L. Williams, H. J. Grill, D. E. Cummings, J. M. Kaplan, Vagotomy dissociates short- and long-term controls of circulating ghrelin. *Endocrinology* **144**, 5184–5187 (2003).
30. A. Shine, T. L. Abell, Role of gastric electrical stimulation in the treatment of gastroparesis. *Gastrointestinal Disorders* **2**, 12–26 (2020).
31. S. Li, J. D. Chen, Pulse width-dependent effects of intestinal electrical stimulation for obesity: Role of gastrointestinal motility and hormones. *Obes. Surg.* **27**, 70–77 (2017).
32. F. Ye, Y. Liu, S. Li, J. D. Z. Chen, Hypoglycemic effects of intestinal electrical stimulation by enhancing nutrient-stimulated secretion of GLP-1 in rats. *Obes. Surg.* **28**, 2829–2835 (2018).
33. Y. Wang, Q. Wang, K. Kuerban, M. Dong, F. Qi, G. Li, J. Ling, W. Qiu, W. Zhang, L. Ye, Colonic electrical stimulation promotes colonic motility through regeneration of myenteric plexus neurons in slow transit constipation beagles. *Biosci. Rep.* **39**, BSR20182405 (2019).
34. X. R. Qin, Y. Tan, X. N. Sun, Effect of retrograde colonic electrical stimulation on colonic transit and stress-induced visceral hypersensitivity in rats with irritable bowel syndrome. *Asian Pac. J. Trop. Med.* **10**, 827–832 (2017).
35. D. Belder, A. Deege, H. Husmann, F. Kohler, M. Ludwig, Cross-linked poly(vinyl alcohol) as permanent hydrophilic column coating for capillary electrophoresis. *Electrophoresis* **22**, 3813–3818 (2001).
36. D. S. Wavhal, E. R. Fisher, Hydrophilic modification of polyethersulfone membranes by low temperature plasma-induced graft polymerization. *J. Membr. Sci.* **209**, 255–269 (2002).
37. G. K. Belmonte, G. Charles, M. C. Strumia, D. E. Weibel, Permanent hydrophilic modification of polypropylene and poly(vinyl alcohol) films by vacuum ultraviolet radiation. *Appl. Surf. Sci.* **382**, 93–100 (2016).
38. J. N. Chu, G. Traverso, Foundations of gastrointestinal-based drug delivery and future developments. *Nat. Rev. Gastroenterol. Hepatol.* **19**, 219–238 (2021).
39. H. Y. Zhang, Y. Wang, S. Vasilescu, Z. B. Gu, T. Sun, Bio-inspired enhancement of friction and adhesion at the polydimethylsiloxane-intestine interface and biocompatibility characterization. *Mater. Sci. Eng. C-Mater. Biol. Appl.* **74**, 246–252 (2017).
40. J. Li, A. D. Celiz, J. Yang, Q. Yang, I. Wamala, W. Whyte, B. R. Seo, N. V. Vasilyev, J. J. Vlassak, Z. Suo, D. J. Mooney, Tough adhesives for diverse wet surfaces. *Science* **357**, 378–381 (2017).
41. W. C. Xie, V. Kothari, B. S. Terry, A bio-inspired attachment mechanism for long-term adhesion to the small intestine. *Biomed. Microdevices* **17**, 68 (2015).
42. M. Mimee, P. Nadeau, A. Hayward, S. Carim, S. Flanagan, L. Jerger, J. Collins, S. McDonnell, R. Swartwout, R. J. Citorik, V. Bulović, R. Langer, G. Traverso, A. P. Chandrakasan, T. K. Lu, An ingestible bacterial-electronic system to monitor gastrointestinal health. *Science* **360**, 915–918 (2018).
43. J. K. Lunney, A. van Goor, K. E. Walker, T. Hailstock, J. Franklin, C. Dai, Importance of the pig as a human biomedical model. *Sci. Transl. Med.* **13**, eabd5758 (2021).
44. M. C. Garin, C. M. Burns, S. Kaul, A. R. Cappola, Clinical review: The human experience with ghrelin administration. *J. Clin. Endocrinol. Metab.* **98**, 1826–1837 (2013).
45. N. M. Neary, C. J. Small, A. M. Wren, J. L. Lee, M. R. Druce, C. Palmieri, G. S. Frost, M. A. Ghatei, R. C. Coombes, S. R. Bloom, Ghrelin increases energy intake in cancer patients with

impaired appetite: Acute, randomized, placebo-controlled trial. *J. Clin. Endocrinol. Metab.* **89**, 2832–2836 (2004).
46. F. Levin, T. Edholm, P. T. Schmidt, P. Grybäck, H. Jacobsson, M. Degerblad, C. Höybye, J. J. Holst, J. F. Rehfeld, P. M. Hellström, E. Näslund, Ghrelin stimulates gastric emptying and hunger in normal-weight humans. *J. Clin. Endocrinol. Metab.* **91**, 3296–3302 (2006).
47. G. Iddan, G. Meron, A. Glukhovsky, P. Swain, Wireless capsule endoscopy. *Nature* **405**, 417–417 (2000).
48. S. Sharma, K. B. Ramadi, N. H. Poole, S. S. Srinivasan, K. Ishida, J. Kuosmanen, J. Jenkins, F. Aghlmand, M. B. Swift, M. G. Shapiro, G. Traverso, A. Emami, Location-aware ingestible microdevices for wireless monitoring of gastrointestinal dynamics. *Nat. Electron.* **6**, 242–256 (2023).
49. Y. Mintz, S. Horgan, M. K. Savu, J. Cullen, A. Chock, S. Ramamoorthy, D. W. Easter, M. A. Talamini, Hybrid natural orifice translumenal surgery (NOTES) sleeve gastrectomy: A feasibility study using an animal model. *Surg. Endosc.* **22**, 1798–1802 (2008).
50. M. Tarnoff, S. Shikora, A. Lembo, Acute technical feasibility of an endoscopic duodenal-jejunal bypass sleeve in a porcine model: A potentially novel treatment for obesity and type 2 diabetes. *Surg. Endosc.* **22**, 772–776 (2008).

Acknowledgments: We acknowledge the assistance of the histology core of the Koch Institute for Integrative Cancer Research, supported in part by the National Cancer Institute (P30-CA14051 to the Koch Institute Core). We thank V. E. Fulford, Alar Illustration for work in Figs. 1 and 2. **Funding:** K.B.R. was supported by the National Institute of Diabetes and Digestive and Kidney Diseases (NIDDK) of the National Institutes of Health (NIH) under award number F32DK122762 and the Division of Engineering at NYU Abu Dhabi. J.C.M. was supported in part by an NSF Graduate Research fellowship. This work was supported in part by Novo Nordisk, the Karl van Tassel (1925) Career Development Professorship, and the Department of Mechanical Engineering at MIT. **Author contributions:** K.B.R., J.C.M., and G.T. developed the concept, shape, and device. G.S. developed the electronics. J.C.M. characterized in vitro functionality. K.B.R., J.C.M., N.X.-J.J., K.I., J.K., J.J., and A.H. performed animal studies. A.A. and S.M. assisted with device fabrication and manufacturing. A.S., R.F., M.H., and B.R. performed hormone analyses and device preparation. S.B. conducted computational modeling. K.B.R. created figures. K.B.R., K.K., and G.T. supervised the project. G.T. acquired funding. K.B.R., J.C.M., and G.T. wrote the paper with contributions from K.K. All authors discussed results and edited the manuscript. **Competing interests:** K.B.R., J.C.M., and G.T. are co-inventors on a patent application (no. 63/092,016) encompassing the work described. Complete details of all relationships for profit and not for profit for G.T. can be found at the following link: www.dropbox.com/sh/szi7vnr4a2ajb56/AABs5N5i0q9AfT1IqIJAE-T5a?dl=0. **Data and materials availability:** All data needed to evaluate the conclusions in the paper are present in the paper or in the Supplementary Materials.

Submitted 20 September 2022
Accepted 29 March 2023
Published 26 April 2023
10.1126/scirobotics.ade9676

Science Robotics

Bioinspired, ingestible electroceutical capsules for hunger-regulating hormone modulation

Khalil B. Ramadi, James C. McRae, George Selsing, Arnold Su, Rafael Fernandes, Maela Hickling, Brandon Rios, Sahab Babaee, Seokkee Min, Declan Gwynne, Neil Zixun Jia, Aleyah Aragon, Keiko Ishida, Johannes Kuosmanen, Josh Jenkins, Alison Hayward, Ken Kamrin, and Giovanni Traverso

Sci. Robot. **8** (77), eade9676. DOI: 10.1126/scirobotics.ade9676

Science Robotics (ISSN 2470-9476) is published by the American Association for the Advancement of Science. 1200 New York Avenue NW, Washington, DC 20005. The title *Science Robotics* is a registered trademark of AAAS.